Digital Post-Distortion for Multi-Layer MIMO-OFDM

Huseyin Babaroglu, Lauri Anttila, Guixian Xu, and Mikko Valkama, *Fellow, IEEE*

Abstract—In this letter, we propose a new digital post-distortion (DPoD) technique for precoded multi-layer orthogonal frequency division multiplexing (OFDM) systems, in order to enhance the received signal error vector magnitude (EVM) under heavily nonlinear power amplifiers (PAs) in the transmitter. The proposed multi-layer digital post-inverse (ML-DPoI) builds on layer- or stream-level nonlinear distortion modeling and corresponding signal processing at receiver, combined with true reference signal based model parameter estimation allowing to operate without any prior knowledge of the transmit precoder or PA behavior. Numerical evaluations with dual-layer rank-2 transmission in 5G New Radio (NR) uplink context with standard-compatible physical-layer transmit waveform show that despite heavily nonlinear PA units, the received signal EVM can be reliably enhanced – even in the case of very high modulation order such as 256-QAM per transmit stream. These results pave the way towards improved power-efficiency and sustainability in future networks, especially at millimeter-wave bands, where transmitter power-efficiency is known to be a major implementation challenge.

Index Terms—5G, 6G, digital post-distortion, EVM, DMRS, MIMO-OFDM, multi-layer precoding, nonlinear distortion, physical-layer, power amplifier, power-efficiency, RF impairments

I. INTRODUCTION

THE HIGH peak-to-average power ratio (PAPR) of orthogonal frequency division multiplexing (OFDM) waveforms creates a fundamental tradeoff between the transmitter (TX) power-efficiency and the antenna signal quality when operating under practical nonlinear power amplifiers (PAs) [1]. Different digital predistortion (DPD) methods are the most established approach to suppress PA nonlinear distortion, especially in cellular base-stations (BSs). However, applying DPD in emerging millimeter-wave (mmWave) networks with increasing bandwidths, large amounts of PA units, and elaborate hybrid beamforming methods is known to be challenging [2]. Additionally, in *cellular uplink*, the processing capabilities of user equipment (UE) and thereon the prospects of using DPD are much more limited compared to base-stations.

Digital post-distortion (DPoD) [3], [4] is an alternative, *receiver-based method* to suppress transmitter PA distortion, with primary emphasis on inband signal quality and improving the corresponding error vector magnitude (EVM). This is also the main technical scope of this letter, with specific focus on cellular uplink and challenging pre-coded multi-layer transmission with high modulation order per transmit stream.

Different means for improved energy-efficiency, including DPoD, are also currently considered in 3GPP standardization for the evolution of 5G New Radio (NR) [5], while a notable energy-efficiency leap and the overall sustainability are among the key targets towards IMT-2030 and 6G [6].

The seminal model-based works in [3], [4] introduce the so-called PA nonlinearity cancellation (PANC) and reconstruction of distorted signals (RODS) methods, respectively, in ordinary single-antenna or single-stream system context. Further single-stream refinements are provided, e.g., in [7], [8], while [9] develops machine learning (ML) based physical-layer receiver for single-stream OFDM transmission showing robustness against PA distortion. Additionally, different multiantenna or MIMO variants have been considered in [10], [11], [12], [13], [14], [15], [16], [17]. In [10], [12], transmission of multiple parallel streams is assumed, however, channel-aware transmit precoding is not considered and the TX nonlinearity is assumed known. In [11], in turn, rank-1 space-time coded transmission is considered while again assuming a known TX nonlinearity at receiver. In [13], a multi-user MIMO case is considered with rank-1 transmission per UE, hence neglecting nonlinear mixing or interference between the streams. The work in [14] considers again rank-1 transmission and proposes new pilot or reference signal structures for nonlinear TX model estimation. In [15], space-frequency transmit diversity system is considered under the assumption of known channel and TX nonlinearity. In [16], an iterative receiver scheme is devised for multi-layer transmission, assuming a known TX nonlinearity. The work in [17] considers hybrid beamforming based MIMO system and devises an iterative particle-filter based receiver solution building again on the assumption of a known TX nonlinearity. Importantly, in all of the above works, the fundamental aspect of TX nonlinearity model estimation at receiver is neglected, while many being also applicable only in rank-1 transmission scenarios, missing the channel-aware precoding aspects, or calling for iterative processing with notable complexity. Hence, in this letter, we bridge these important gaps and focus on pre-coded multi-layer transmissions beyond rank-1, and provide a direct one-shot DPoD solution referred to as the multi-layer digital post-inverse (ML-DPoI) while also explicitly consider the TX nonlinearity model estimation using the available reference signals. First, multi-dimensional baseband nonlinearity modeling is provided, describing how a PA nonlinearity with precoded signals is impacting at stream-level. Inspired by the modeling, the proposed one-shot ML-DPoI scheme is then devised, being complemented with demodulation reference signal (DMRS) based parameter estimation scheme. Finally, comprehensive numerical results are provided in the context of 5G NR dual-layer rank-2 uplink transmission at 28 GHz mmWave band with standard-compliant uplink waveform and DMRS structure. The obtained results show that despite heavily nonlinear PA units at UE, the received signal EVM can be reliably enhanced through the proposed DPoD scheme even in the very challenging case of 256-QAM data modulation.

II. SYSTEM MODEL

We consider an $N_{\mathrm{TX}} \times N_{\mathrm{RX}}$ MIMO-OFDM transmission system with N_{L} parallel streams where N_{TX} and N_{RX} denote the numbers of transmit and receive antennas, respectively. The transmit symbol of stream i at subcarrier k is denoted by $a_k^{(i)}$, with $k \in \{-N_{\mathrm{act}}/2, \ldots, N_{\mathrm{act}}/2 - 1\}$, $i \in \{1, 2, \ldots, N_{\mathrm{L}}\}$, while N_{act} denotes the number of active subcarriers. The data symbols of the transmission layers are mapped to transmit antennas via precoding, expressed in vector matrix format as

$$\mathbf{s}_k = \mathbf{V}\mathbf{a}_k, \tag{1}$$

where $\mathbf{a}_k = [a_k^{(1)}, a_k^{(2)}, \ldots, a_k^{(N_{\mathrm{L}})}]^T$ is the $N_{\mathrm{L}} \times 1$ data vector, $\mathbf{V}$ is the $N_{\mathrm{TX}} \times N_{\mathrm{L}}$ precoding matrix, and $\mathbf{s}_k = [s_k^{(1)}, s_k^{(2)}, \ldots, s_k^{(N_{\mathrm{TX}})}]^T$ is the $N_{\mathrm{TX}} \times 1$ precoded antenna signal vector. We note that frequency-independent precoding is deliberately considered, as such approach is the baseline method in 5G NR uplink [18].

While the precoding is commonly implemented in frequency-domain, as shown in (1), we next express the equivalent time-domain model which then allows for including PA nonlinear distortion modeling through well-established models such as the memory polynomial (MP) [19]. To this end, the time-domain equivalent of (1) can be directly expressed as

$$x^{(j)}(n) = \sum_{i=1}^{N_{\mathrm{L}}} v_{ji} z^{(i)}(n), \tag{2}$$

where $z^{(i)}(n)$, and $x^{(j)}(n)$ denote the discrete-time OFDM waveform samples corresponding to $a_k^{(i)}$ and $s_k^{(j)}$, respectively, while v_{ji} denote the entries of the precoding matrix $\mathbf{V}$. To accommodate accurate PA modeling, we assume that the time-domain model sample rate is $f_s = \varepsilon N_{\mathrm{FFT}} \Delta f$, where ε is the oversampling factor, N_{FFT} is the fundamental OFDM fast Fourier transform (FFT) size, and Δf denotes the subcarrier spacing (SCS). Thus, assuming further that the cyclic prefix (CP) length is N_{CP}, $z^{(i)}(n)$ can be expressed as

$$z^{(i)}(n) = \frac{1}{\sqrt{N}} \sum_{k=-N_{\mathrm{act}}/2}^{N_{\mathrm{act}}/2-1} a_k^{(i)} e^{j2\pi kn/N}, \quad -N_{\mathrm{CP}} \le n \le N-1, \tag{3}$$

where $N = \varepsilon N_{\mathrm{FFT}}$, while the corresponding samples of $x^{(j)}(n)$ follow through (2).

To now explicitly account for the TX nonlinearities, we employ the widely-used memory polynomial (MP) modeling approach [19]. It is further assumed that each transmit antenna branch has its own individual nonlinear PA unit. The corresponding nonlinearly distorted transmit waveform on j-th antenna branch, $y^{(j)}(n)$, can now be expressed as

$$y^{(j)}(n) = \sum_{\substack{p=1 \\ p \text{ odd}}}^{P_{\mathrm{TX}}} \sum_{d=0}^{D_{\mathrm{TX}}} c_{p,d}^{(j)} x^{(j)}(n-d) \left| x^{(j)}(n-d) \right|^{p-1}, \tag{4}$$

where $c_{p,d}^{(j)}$ is the MP complex coefficient of order p and delay d while P_{TX} and D_{TX} denote the maximum nonlinearity order and memory depth, respectively. Importantly, because of the precoding in (2) and assuming nontrivial precoders with $v_{ji} \neq 0 \; \forall i, j$, an individual *PA input* comprises linear combinations of the individual streams or layers, and thus the nonlinear distortion model in (4) causes a complicated nonlinear distortion profile at *PA output* from the data layers point of view. This is further elaborated in Section III, forming also the basis of the proposed DPoD method.

Next, the distorted antenna waveforms propagate through a noisy MIMO multipath channel. We assume that the receiver basic sample rate is $f_{s,\mathrm{RX}} = N_{\mathrm{FFT}} \Delta f$, and that the receiver front-end contains applicable channel selection filtering. The corresponding channel-filtered received signal is transformed at the receiver into frequency domain via FFT of size N_{FFT}. The resulting frequency-domain samples at subcarrier k across the RX antennas can be expressed in vector-matrix notation as

$$\mathbf{R}(k) = \mathbf{H}(k)\mathbf{Y}_{\mathrm{filt}}(k) + \mathbf{W}_{\mathrm{filt}}(k), \tag{5}$$

where $\mathbf{H}(k)$ is the $N_{\mathrm{RX}} \times N_{\mathrm{TX}}$ MIMO channel frequency response matrix at subcarrier k. Furthermore, $\mathbf{Y}_{\mathrm{filt}}(k)$ stacks the FFT values of the effective channel-filtered transmit antenna waveforms at subcarrier k, while $\mathbf{W}_{\mathrm{filt}}(k)$ refers to the corresponding FFT values of the channel-filtered thermal noise at subcarrier k.

Finally, we assume that ordinary linear minimum mean-squared error (LMMSE) equalizer is employed to mitigate the MIMO channel linear distortion. We further assume that the uplink reference signal transmissions are also precoded [18], such that the RX can estimate directly the effective pre-coded linear channel without TX precoder knowledge. We express the effective precoded MIMO channel as $\mathbf{H}_{\mathrm{eff}}(k) = \mathbf{H}_{\mathrm{cs}}(k)\mathbf{H}(k)\mathbf{V}$, where the diagonal matrix $\mathbf{H}_{\mathrm{cs}}(k)$ accounts for the frequency responses of the channel selection filters at RX branches. Denoting further the corresponding equalizer of size $N_{\mathrm{L}} \times N_{\mathrm{RX}}$ by $\mathbf{H}_{\mathrm{eq}}(k)$, the equalizer output signal reads

$$\mathbf{Q}(k) = \mathbf{H}_{\mathrm{eq}}(k)\mathbf{H}(k)\mathbf{Y}_{\mathrm{filt}}(k) + \mathbf{H}_{\mathrm{eq}}(k)\mathbf{W}_{\mathrm{filt}}(k). \tag{6}$$

This equalizer output serves as the input to the proposed DPoD processing, described next. Furthermore, the fundamental considered system model is graphically illustrated in Fig. 1.

III. PROPOSED METHODS

A. Multi-Input Baseband Nonlinearity Modeling

We start by explicitly addressing the nonlinear system model at layer or stream level, building on the antenna waveform model in (4). By substituting the precoded signal expression in (2) into (4), we can first formally write

$$y^{(j)}(n) = \sum_{\substack{p=1 \\ p \text{ odd}}}^{P_{\mathrm{TX}}} \sum_{d=0}^{D_{\mathrm{TX}}} c_{p,d}^{(j)} \Big(v_{j1} z^{(1)}(n-d) + \cdots + v_{jN_{\mathrm{L}}} z^{(N_{\mathrm{L}})}(n-d) \Big)$$
$$\times \left| \Big(v_{j1} z^{(1)}(n-d) + \ldots + v_{jN_{\mathrm{L}}} z^{(N_{\mathrm{L}})}(n-d) \Big) \right|^{p-1}. \tag{7}$$

Next, for notational convenience, let us denote $z^{(i)}(n)$ as z_i while momentarily omitting also the antenna branch index j. Then, (7) can be rewritten for any given antenna index j as

$$y(n) = \sum_{m=1}^{N_{\mathrm{TX}}^{\mathrm{BF}}} \sum_{d=0}^{D_{\mathrm{TX}}} \Upsilon_{m,d}(n) \bar{c}_{m,d}, \tag{8}$$

where $\Upsilon_{m,d}(n) = \Upsilon_m(n-d)$ are the nonlinear basis functions that are now comprised directly of the *unprecoded input layers* z_i. The exact expressions for these basis functions are given below, with further details being available in the Appendix. Furthermore, $\bar{c}_{m,d}$ denote the effective complex coefficients lumping the underlying unknown MP model coefficients $c_{p,d}^{(j)}$ and the precoder weights v_{ji}, while $N_{\mathrm{TX}}^{\mathrm{BF}}$ denotes the number of memoryless basis functions which in general depends on the nonlinearity order P_{TX} and the number of layers N_{L}. The corresponding vector-matrix model for any
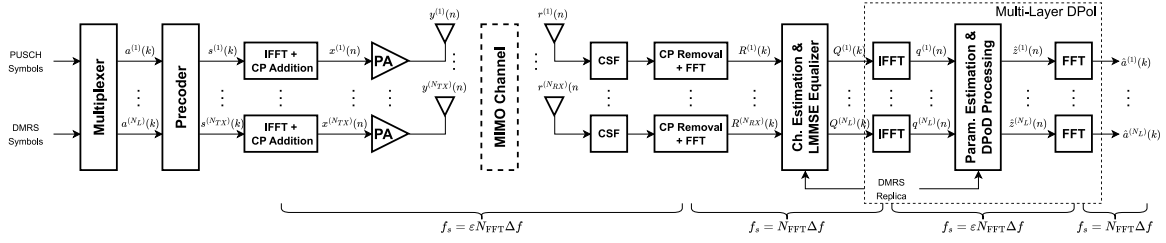
Fig. 1. Baseband equivalent block-diagram of the considered multi-layer MIMO-OFDM system with TX nonlinearities included. Up- and down-sampling are embedded in IFFT/FFT operations, respectively.

given OFDM symbol with N samples (excluding CP) can be expressed as

$$y = \Upsilon \bar{c} \qquad (9)$$

where y is of size $N \times 1$, Υ is the $N \times N_{\text{TX}}^{\text{coef}}$ basis function matrix, and $\bar{c}$ is the $N_{\text{TX}}^{\text{coef}} \times 1$ coefficient matrix, with $N_{\text{TX}}^{\text{coef}} = N_{\text{TX}}^{\text{BF}}(D_{\text{TX}} + 1)$ denoting the total number of coefficients.

The exact expressions for the nonlinear basis function samples $\Upsilon_{m,d}(n)$ can basically be solved through brute-force, by working out the substitution in (7) for a given nonlinearity order P_{TX}. To address this more elegantly for an arbitrary nonlinearity order, we next introduce a recursive approach to obtain the entries of the basis function matrix Υ. To this end, let us denote the set of *instantaneous basis functions* that corresponds to a nonlinearity order of p as $\Upsilon^{(p)}$, for any arbitrary sample instant n. Now, stemming from the nature of the assumed memory polynomial PA model, a recursive relation can be established between orders p and $p-2$, expressed as

$$\bar{\Upsilon}^{(p)} = \Upsilon^{(p-2)} \otimes \mathbf{G}, \qquad (10)$$

where $\otimes$ denotes the Kronecker product, $\mathbf{G}$ is a *generator vector*, while the fundamental linear basis function set is defined as $\Upsilon^{(1)} = [z_1(n), z_2(n), \ldots, z_{N_{\text{L}}}(n)]^T$. The entries of the generator vector $\mathbf{G}(n)$ contain all pairwise products of the involved streams with the other element always complex-conjugated. Concrete example for $N_{\text{L}} = 2$ is available in the Appendix. Furthermore, and importantly, the recursion in (10) provides always the correct basis function terms but includes also some duplicates when directly implemented. Thus, the actual basis function set $\Upsilon^{(p)}$ is obtained from $\bar{\Upsilon}^{(p)}$ in (10) by simply removing the repetitive terms. An example for $N_{\text{L}} = 2$ is given in the Appendix.

B. Multi-Layer Digital Post-Inverse (ML-DPoI)

Building on the previous modeling, we next describe the actual proposed multi-layer DPoD processing operating at RX. First, the LMMSE equalizer output in (6) is transformed back to time-domain for more efficient calculation of nonlinear transformations. This is done via $N = \varepsilon N_{\text{FFT}}$ -point IFFT, and yields a signal $q^{(i)}(n)$ for the i-th layer, expressed as

$$q^{(i)}(n) = \tilde{y}^{(i)}(n) + \tilde{w}^{(i)}(n), \qquad (11)$$

where $\tilde{y}^{(i)}(n)$ and $\tilde{w}^{(i)}(n)$ denote the upsampled time-domain sequences of the first and the second terms in (6).

Now, the actual multi-layer DPoD processing, referred to as the multi-layer digital post-inverse (ML-DPoI), is based on a processing engine similar to the transmitter nonlinearity modeling in (8), in which the inputs are the received and equalized time-domain layers $q^{(i)}(n)$ in (11). That is, the basis functions up to order P_{RX} are calculated using the

time-domain layers $q^{(i)}(n)$, while because of seeking inverse nonlinearities, we denote the corresponding basis functions with Υ_{inv} in the following. Thus, the ML-DPoI output for layer i is defined as

$$\hat{z}^{(i)}(n) = \sum_{m=1}^{N_{\text{RX}}^{\text{BF}}} \sum_{d=0}^{D_{\text{RX}}} \Upsilon_{\text{inv},m,d} \theta_{m,d}^{(i)} \qquad (12)$$

where $\theta_{m,d}^{(i)}$ denote the ML-DPoI processing coefficients. Similar to (9), and to support efficient parameter estimation, it is convenient to represent (12) in vector-matrix notation. Accounting for all involved N_{L} parallel layers, we express this as

$$\hat{\mathbf{Z}} = \Upsilon_{\text{inv}} \theta, \qquad (13)$$

where $\hat{\mathbf{Z}}$ denotes the $N \times N_{\text{L}}$ post-distorter output matrix with one column representing one layer, Υ_{inv} is the $N \times N_{\text{RX}}^{\text{coef}}$ basis function matrix, θ is the $N_{\text{RX}}^{\text{coef}} \times N_{\text{L}}$ matrix of the inverse model coefficients, and $N_{\text{RX}}^{\text{coef}} = N_{\text{RX}}^{\text{BF}}(D_{\text{RX}} + 1)$. Finally, the output signals $\hat{z}^{(i)}(n)$ are decimated by ε and transformed via N_{FFT}-point FFT for the actual bit or symbol detection.

C. DMRS-Based Parameter Estimation

Next, we address the DMRS-based estimation of the *inverse model parameters* θ. This is important since in real networks, the PA model coefficients are unknown at RX. Additionally, when DMRS transmission is precoded similar to data symbols [18], the receiver does not know the applied precoding weights either. However, the precoded DMRS symbols form direct basis for effective linear channel estimation as well as estimation of the ML-DPoI model parameters in (13). The linear channel estimation is a standard procedure, while the parameter estimation for the proposed ML-DPoI is one technical contribution of this letter. To this end, by using the known DMRS sequences, $z_{\text{ref}}^{(i)}(n)$, as the basis, we can write

$$\mathbf{Z}_{\text{ref}} = \Upsilon_{\text{ref}} \theta, \qquad (14)$$

where $\mathbf{Z}_{\text{ref}}$ is an $N \times N_{\text{L}}$ matrix with columns representing $z_{\text{ref}}^{(i)}(n)$ for $i = 1, 2, \ldots, N_{\text{L}}$, Υ_{ref} is the $N \times N_{\text{RX}}^{\text{coef}}$ basis function matrix during DMRS reception, and θ is the $N_{\text{RX}}^{\text{coef}} \times N_{\text{L}}$ matrix of inverse model coefficients. Then, the unknown coefficient matrix can be estimated with least-squares (LS) as

$$\theta = \left(\Upsilon_{\text{ref}}^H \Upsilon_{\text{ref}} \right)^{-1} \Upsilon_{\text{ref}}^H \mathbf{Z}_{\text{ref}}. \qquad (15)$$

D. Notes on Complexity

We next shortly address the ML-DPoI processing complexity. Building directly on the basis function generation

TABLE I
EXAMPLE AMOUNTS OF MEMORYLESS BASIS FUNCTIONS ($N_{\mathrm{RX}}^{\mathrm{BF}}$)

P_{RX}	$N_{\mathrm{L}} = 2$	$N_{\mathrm{L}} = 3$	$N_{\mathrm{L}} = 4$
1	2	3	4
3	8	21	44
5	20	81	244
7	40	231	944
9	70	546	2904

TABLE II
EXAMPLE AMOUNTS OF FLOPs PER SAMPLE TO EXECUTE
ML-DPoI, EXCLUDING IFFT/FFT

P_{RX}	$N_{\mathrm{L}} = 2$	$N_{\mathrm{L}} = 3$	$N_{\mathrm{L}} = 4$
3	$128D_{\mathrm{RX}} + 180$	$504D_{\mathrm{RX}} + 678$	$1408D_{\mathrm{RX}} + 1816$
5	$320D_{\mathrm{RX}} + 468$	$1944D_{\mathrm{RX}} + 2874$	$7808D_{\mathrm{RX}} + 11416$
7	$640D_{\mathrm{RX}} + 980$	$5544D_{\mathrm{RX}} + 8994$	$30208D_{\mathrm{RX}} + 49816$
9	$1120D_{\mathrm{RX}} + 1780$	$13104D_{\mathrm{RX}} + 22854$	$92928D_{\mathrm{RX}} + 168536$

mechanism in (10), the numbers of instantaneous basis functions, $N_{\mathrm{RX}}^{\mathrm{BF}}$, can be deduced and are shown in Table I for feasible example values of P_{RX} and N_{L}. The corresponding actual floating point operations (FLOPs) per processed sample, excluding the IFFT/FFT operations, can also be calculated. These are provided in Table II. One can clearly observe that the complexity grows fast for increasing P_{RX}, especially if $N_{\mathrm{L}} > 2$. However, for $N_{\mathrm{L}} = 2$, the complexity numbers are still modest even for fairly large values of P_{RX}.

IV. NUMERICAL RESULTS

The proposed ML-DPoI method is next evaluated in a computer simulation environment using MATLAB, while focusing on the practical case of dual-layer transmission ($N_{\mathrm{L}} = 2$). Random realizations of 5G NR standard-compliant uplink CP-OFDM waveform of length 14 OFDM symbols (1 slot) are used. The assumed values of the different related parameters and quantities are listed in Table III. Furthermore, the layer-to-antenna mapping of data symbols and DMRS is performed assuming a codebook-based transmission as described in [20], with a randomly chosen transmit precoding matrix indicator (TPMI) value (within nontrivial precoders corresponding to TPMI values from 14 to 21 defined in [20]), while DMRS boosting is employed as described in [7]. Each transmit branch has its own PA unit whose nonlinear behaviors are characterized by measured MP models available in [21] with mutually different coefficient realizations. A soft envelope limiter is also deployed, such that the PAPR of the PA input signal is limited to 8 dB. The strength of nonlinearity introduced by the PAs is controlled with the back-off applied at the PA input, ranging from 4.25 dB to 9.25 dB with 0.5 dB increments. In exact terms, the input backoff is defined as

$$\mathrm{IBO[dB]} = 10\log_{10}\left(P_{\mathrm{in\text{-}sat}}/P_{\mathrm{avg}}\right), \tag{16}$$

where $P_{\mathrm{in\text{-}sat}}$ and P_{avg} are the input saturation power of the PA and the average power of the PA input signal, respectively. The assumed reference input saturation power of an individual PA module is $+5$ dBm.

The involved 4×64 MIMO multipath channel is modeled by CDL-E channel profile [22] with RMS delay spread (DS) of 43 ns. LMMSE equalizer with practical DMRS-based linear channel estimate is employed before ML-DPoI, as shown also in Fig. 1. Both the linear channel and the ML-DPoI parameter

TABLE III
NUMERICAL EVALUATION PARAMETERS AT 28 GHz

Parameter	Value	Parameter	Value
Modulation	256-QAM	$P_{\mathrm{TX}}, D_{\mathrm{TX}}$	11, 5
$N_{\mathrm{act}}, N_{\mathrm{L}}$	3168, 2	$P_{\mathrm{RX}}, D_{\mathrm{RX}}$	5, 5
Δf	60 kHz	$N_{\mathrm{TX}}, N_{\mathrm{RX}}$	4, 64
N_{FFT}	4096	SNR	30 dB
ε	5	RMS DS	43 ns

TABLE IV
EVM PERFORMANCE WITH DOUBLE-DMRS FOR TWO EXAMPLE IBO
VALUES WHILE VARYING P_{RX} FOR ML-DPoI

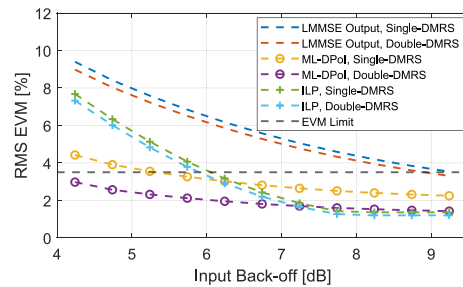| IBO [dB]	LMMSE Output	$P_{\mathrm{RX}} = 3$	$P_{\mathrm{RX}} = 5$	$P_{\mathrm{RX}} = 7$	$P_{\mathrm{RX}} = 9$
4.25	8.88%	4.01%	2.96%	3.01%	3.44%
5.25	7.21%	3.16%	2.39%	2.42%	2.87%

Fig. 2. FR2 EVM performance results at 28 GHz with 200 MHz channel bandwidth, CDL-E multipath channel, and 256-QAM data modulation.

estimation are executed on per-slot basis, using DMRS. The main performance metric is the received signal EVM for PUSCH symbols – with thermal noise excluded from the EVM calculation to focus on the true useful signal quality under the noise. Thermal noise is, however, properly modelled in all other stages, such as the LMMSE and ML-DPOI parameter estimation phases, for realistic assessments. Since the existing literature does not contain any model-based RX DPoD reference methods applicable for true multi-layer transmission with unknown transmitter nonlinearities, the performance of the proposed method is compared to that of an ideally linearized PA (ILP), which has a constant gain over its linear range while entering saturation after $P_{\mathrm{in\text{-}sat}}$ is reached.

Figure 2 shows the achieved receiver EVM values of the proposed ML-DPoI and of the LMMSE and ILP benchmarks with 256-QAM. Compared to the ordinary LMMSE, employing ML-DPoI provides substantial EVM enhancements. Specifically, when *single-symbol DMRS* is utilized for parameter estimation, the tight EVM limit is satisfied at and above 5.25 dB IBO values, reflecting an IBO gain of around 4 dB compared to ordinary LMMSE. Additionally, the receiver EVM is consistently below the required EVM limit when *double-symbol DMRS* is utilized, corresponding to even larger IBO gains of more than 5 dB. It can also be observed that the proposed ML-DPoI shows better performance compared to the corresponding ILP benchmark at the important low IBO region. This is due to the fact that the PA input signal has a high PAPR, and thus when the IBO is low, significant amounts of samples are essentially tending towards the clipping or saturation region. The number of such samples gradually decreases with increasing IBO, and the ILP starts to eventually perform better than ML-DPoI. These results thus directly show that the ML-DPoI is capable of satisfying tight EVM

requirements at the challenging low IBO values where the *ideally linearized PA approach already fails*. This implies that the ML-DPoI allows for higher power-efficiency by letting the PAs operate in their highly nonlinear region.

Setting the ML-DPoI nonlinearity order is, in general, a compromise between modeling capability and processing complexity. However, as illustrated in Table IV, large EVM improvements can already be obtained with modest orders of $P_{RX} = 3$ and $P_{RX} = 5$ – even when operating at low IBOs. In this case, increasing the nonlinearity order beyond $P_{RX} = 5$ does not further improve the performance. However, it is important to acknowledge that the exact optimization of the involved nonlinearity order and memory depth is always eventually subject to the made assumptions and thus application specific.

V. CONCLUSION

In this letter, we proposed a new digital post-distortion technique for precoded multi-layer MIMO-OFDM systems under strong transmitter nonlinear distortion. The proposed ML-DPoI builds on a layer-level nonlinear distortion modeling and consists of reference signal based model parameter estimation and the corresponding receiver side post-processing. Furthermore, ML-DPoI is a one-shot approach and it does not require any prior information of the transmit precoder or PA model parameters. The performance of the proposed method was evaluated through computer simulations considering a dual-layer 5G NR mmWave uplink transmission at 28 GHz. The results showed that employing ML-DPoI provides significant enhancements in the receiver EVM, and is able to meet the tight EVM limit of 3.5% standardized for 256-QAM at low IBO values. It was also shown that the proposed method outperforms an ideally linearized transmitter at low IBO values, allowing transmitter PAs to operate in their highly nonlinear but power-efficient region while still fulfilling the corresponding EVM limits. Our future work focuses on extending the proposed method to frequency-selective precoding scenarios.

APPENDIX

INSTANTANEOUS BASIS FUNCTION GENERATION

In the following, a concrete BF generation example for $N_L = 2$ with linear basis function set of $\mathbf{\Upsilon}^{(1)} = [z_1(n), z_2(n)]^T$ is given. First, the generator vector reads

$$\mathbf{G} = [|z_1(n)|^2, |z_2(n)|^2, z_1(n)z_2^*(n), z_1^*(n)z_2(n)]^T. \quad (17)$$

Then, for $p = 3$, we can write $\bar{\mathbf{\Upsilon}}^{(3)} = \mathbf{\Upsilon}^{(1)} \otimes \mathbf{G}$ which yields

$$\begin{aligned}
\bar{\mathbf{\Upsilon}}^{(3)} = [&z_1(n)|z_1(n)|^2, \; z_1(n)|z_2(n)|^2, \; z_1(n)z_1(n)z_2^*(n), \\
&z_1(n)z_1^*(n)z_2(n), \; z_2(n)|z_1(n)|^2, \; z_2(n)|z_2(n)|^2, \\
&z_2(n)z_1(n)z_2^*(n), \; z_2(n)z_1^*(n)z_2(n)]^T. \quad (18)
\end{aligned}$$

In above, the fourth item $z_1(n)z_1^*(n)z_2(n)$ is equal to $z_2(n)|z_1(n)|^2$, which is identical to the fifth item. Furthermore, the seventh item $z_2(n)z_1(n)z_2^*(n)$ equals $z_1(n)|z_2(n)|^2$, which is identical to the second item. Thus, $\mathbf{\Upsilon}^{(3)}(n)$ is obtained by removing these duplicate terms, resulting eventually in

$$\begin{aligned}
\mathbf{\Upsilon}^{(3)} = [&z_1(n)|z_1(n)|^2, \; z_1(n)|z_2(n)|^2, \; z_1(n)z_1(n)z_2^*(n), \\
&z_2(n)|z_1(n)|^2, \; z_2(n)|z_2(n)|^2, \; z_2(n)z_1^*(n)z_2(n)]^T. \quad (19)
\end{aligned}$$

The corresponding sets for $p = 5$, $p = 7$ and so forth can be obtained through (10), conceptually similar to above.

REFERENCES

[1] Y. Rahmatallah and S. Mohan, "Peak-to-average power ratio reduction in OFDM systems: A survey and taxonomy," *IEEE Commun. Surveys Tuts.*, vol. 15, no. 4, pp. 1567–1592, 4th Quart., 2013.

[2] C. Fager et al., "Linearity and efficiency in 5G transmitters: New techniques for analyzing efficiency, linearity, and linearization in a 5G active antenna transmitter context," *IEEE Microw. Mag.*, vol. 20, no. 5, pp. 35–49, May 2019.

[3] J. Tellado et al., "Maximum-likelihood detection of nonlinearly distorted multicarrier symbols by iterative decoding," *IEEE Trans. Commun.*, vol. 51, no. 2, pp. 218–228, Feb. 2003.

[4] Z. Alina and O. Amrani, "On digital post-distortion techniques," *IEEE Trans. Signal Process.*, vol. 64, no. 3, pp. 603–614, Feb. 2016.

[5] "Study on network energy savings for NR (Release 18)," 3GPP, Sophia Antipolis, France, Rep. 38.864, V18.0.0, Dec. 2022.

[6] *Framework and Overall Objectives of the Future Development of IMT for 2030 and Beyond*, Rec. ITU-R M.2160-0, ITU, Geneva, Switzerland, Nov. 2023.

[7] H. Babaroglu et al., "Cellular digital post-distortion: Signal processing methods and RF measurements," in *Proc. IEEE WAMICON*, 2023, pp. 25–28.

[8] J. Guerreiro et al., "Optimum and sub-optimum receivers for OFDM signals with strong nonlinear distortion effects," *IEEE Trans. Commun.*, vol. 61, no. 9, pp. 3830–3840, Sep. 2013.

[9] J. Pihlajasalo et al., "Deep learning OFDM receivers for improved power efficiency and coverage," *IEEE Trans. Wireless Commun.*, vol. 22, no. 8, pp. 5518–5535, Aug. 2023.

[10] M. C. Dakhli et al., "Theoretical analysis and compensation for the joint effects of HPA nonlinearity and RF crosstalk in VBLAST MIMO-OFDM systems over rayleigh fading channel," *EURASIP J. Wireless Commun. Netw.*, vol. 2014, p. 61, Apr. 2014.

[11] A. E. Jayati et al., "Iterative receiver compensation of HPA nonlinearity in MIMO-GFDM system," *Int. J. Intell. Eng. Syst.*, vol. 13, no. 4, pp. 260–270, 2020.

[12] M. C. Dakhli et al., "A theoretical characterization and compensation of nonlinear distortion effects and performance analysis using polynomial model in MIMO OFDM systems under rayleigh fading channel," in *Proc. IEEE ISCC*, 2013, pp. 583–587.

[13] D. Castanheira et al., "Hybrid multiuser equalizer with nonlinearity compensation for wideband mmWave massive MIMO uplink systems," *IEEE Trans. Wireless Commun.*, vol. 21, no. 12, pp. 10286–10299, Dec. 2022.

[14] T. C. Schenk et al., "Receiver-based compensation of transmitter-incurred nonlinear distortion in multiple-antenna OFDM systems," in *Proc. IEEE VTC*, 2007, pp. 1346–1350.

[15] P. Drotar et al., "Receiver based compensation of nonlinear distortion in MIMO-OFDM," in *Proc. IEEE IMWS*, 2010, pp. 1–4.

[16] J. Madeira et al., "Iterative frequency-domain detection for MIMO systems with strong nonlinear distortion effects," in *Proc. IEEE ICUMT*, 2018, pp. 1–5.

[17] P. Priya and D. Sen, "Particle filter based nonlinear data detection in presence of CFO for frequency selective mmWave MIMO-OFDM systems," *IEEE Trans. Veh. Technol.*, vol. 70, no. 6, pp. 5892–5907, Jun. 2021.

[18] *5G Technology: 3GPP New Radio*, 1st ed., H. Holma, A. Toskala, and T. Nakamura, Eds. Hoboken, NJ, USA: Wiley, 2019.

[19] H. Ku and J. Kenney, "Behavioral modeling of nonlinear RF power amplifiers considering memory effects," *IEEE Trans. Microw. Theory Techn.*, vol. 51, no. 12, pp. 2495–2504, Dec. 2003.

[20] "Physical channels and modulation (release 17)," 3GPP, Sophia Antipolis, France, Rep. 38.211, V18.0.0, Sep. 2023.

[21] A. Brihuega et al., "Digital predistortion for multiuser hybrid MIMO at mmWaves," *IEEE Trans. Signal Process.*, vol. 68, pp. 3603–3618, 2020.

[22] "Study on channel model for frequencies from 0.5 to 100 GHz (Release 18)," 3GPP, Sophia Antipolis, France, Rep. 38.901, V18.0.0, Mar. 2024.